This article has been accepted for publication in IEEE Transactions on Mobile Computing. This is the author's version which has not been fully edited and content may change prior to final publication. Citation information: DOI 10.1109/TMC.2025.3540667

CamTuner: Adaptive Video Analytics Pipelines via Real-time Automated Camera Parameter Tuning

Sibendu Paul*, Kunal Rao†, Giuseppe Coviello†, Murugan Sankaradas†, Y. Charlie Hu*, Srimat T. Chakradhar†
*Purdue University, {paul90, ychu}@purdue.edu
† NEC Laboratories America, {kunal, giuseppe.coviello, murugs, chak}@nec-labs.com

***Abstract*—In Video Analytics Pipelines (VAP), Analytics Units (AUs) such as object detection and face recognition operating on remote servers rely heavily on surveillance cameras to capture high-quality video streams to achieve high accuracy. Modern network cameras offer an array of parameters that directly influence video quality. While a few of such parameters, *e.g.,* exposure, focus and white balance, are automatically adjusted by the camera internally, the others are not. We denote such camera parameters as non-automated (NAUTO) parameters. In this work, we first show that in a typical surveillance camera deployment, environmental condition changes can have significant adverse effect on the accuracy of insights from the AUs, but such adverse impact can potentially be mitigated by dynamically adjusting NAUTO camera parameters in response to changes in environmental conditions. Second, since most end-users lack the skill or understanding to appropriately configure these parameters and typically use a fixed parameter setting, we present CamTuner, to our knowledge, the first framework that dynamically adapts NAUTO camera parameters to optimize the accuracy of AUs in a VAP in response to adverse changes in environmental conditions. CamTuner is based on SARSA reinforcement learning and it incorporates two novel components: a light-weight analytics quality estimator and a virtual camera that drastically speed up offline RL training. Our controlled experiments and real-world VAP deployment show that compared to a VAP using the default camera setting, CamTuner enhances VAP accuracy by detecting 15.9% additional persons and 2.6%–4.2% additional cars (without any false positives) in a large enterprise parking lot. CamTuner opens up new avenues for elevating video analytics accuracy, transcending mere incremental enhancements achieved through refining deep-learning models.**

***Index Terms*—Video analytics pipelines (VAP), Camera parameter tuning, Reinforcement learning, Virtual camera.**

I. Introduction

Significant progress in machine learning and computer vision techniques for analyzing video streams [32], along with the explosive growth in Internet of Things (IoT), edge computing, and high-bandwidth access networks such as 5G [45], [14], have led to the wide adoption of video analytics systems. Such systems deploy cameras throughout the world to support diverse applications in entertainment, health-care, retail, automotive, transportation, home automation, safety, and security market segments. The global video analytics market is estimated to grow from $5 billion in 2020 to $21 billion by 2027, at a CAGR of 22.70% [21].

A typical video analytics system consists of a video analytics pipeline (VAP) that starts with one or more surveillance cameras capturing live feed of the target environment. These live feeds are sent over a 5G network to servers at the edge of the 5G network where one or more analytics units (AUs) such as object detection, face detection, and face recognition use deep learning models to mine valuable information in the live video streams, as shown in Figure 1. These AUs critically rely on the cameras to capture high-quality real-time video streams in order to achieve high accuracy.

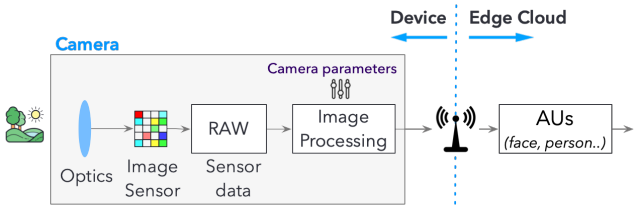

Fig. 1: Standard video analytics pipeline.

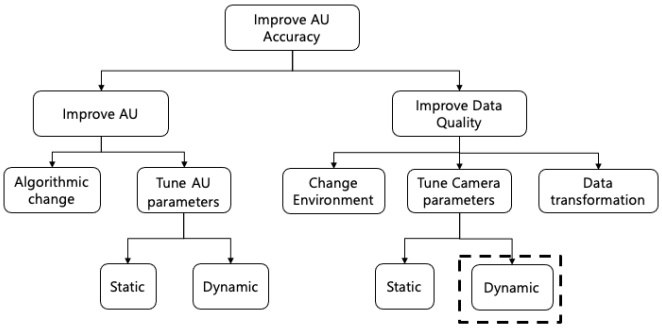

Fig. 2: A taxonomy of techniques for improving AU accuracy in video analytics.

There are two general approaches towards improving the accuracy of an AU in a video analytics system, as shown in Figure 2: improving the AU design and improving the quality of the video stream. In the first approach, one can improve the accuracy of the AU by making algorithmic changes in the underlying DNN model [26], [24], [29], [30], [41]. This, however, is a very expensive and slow reactive solution, because it is not practical to keep training the model with new algorithms and new datasets on costly GPU resources. Another way to improve the AU is by tuning AU parameters, which can be done either at the start, *i.e.,* statically, or during operation, *i.e.,* dynamically. One example of AU parameters is the minimum number of pixels between eyes, which is used for the "face detection" AU. This configurable parameter can be tuned to determine faces in the scene. However, depending on the environmental conditions around the camera (lighting conditions), the content in the scene (number of faces, speed of movement of people), the settings of the camera (brightness,

contrast, color, sharpness, exposure, shutter speed), *etc.*, the quality of the images obtained from the camera can vary. As a result, adjusting the configuration value for "minimum pixels between the eyes" after the image acquisition from the camera may not be able to improve the AU accuracy if the video frame itself is not of good quality.

The second general approach to improving AU accuracy is to improve the quality of data that is fed to the AU. Intuitively, if the AU receives "good" quality input data, *e.g.,* similar to what it has seen during "training", the chance of the AU producing accurate results is high. There are three different ways in which the quality of input data to the AU can be improved, namely, (1) improving the environment around the camera, *e.g.,* by adding additional light in low-light condition, such that the camera is able to get a better capture of the scene, by adding a stabilizer to reduce the camera shake, (2) applying data transformations such as adjustments in compression quality, resolution, or frame appearance (e.g., brightness, contrast *etc.*) on individual frames of the video feed captured by the camera [27], [56], [57], and (3) tuning camera parameters in order to help the camera capture good quality videos. Changing the environment may not be practical in many scenarios and applying data transformation is typically too late because the camera has already captured the scene. However, applying post-capture transformations is fundamentally different from directly modifying camera parameters for better image capture (as in CAMTUNER). Specifically, if the image captured by the camera is of poor quality due to suboptimal camera settings, no subsequent transformations of the video stream can enhance the accuracy of analytics, as demonstrated in Section IX.

Our approach on directly tuning camera parameters is motivated by two observations: (1) Modern IP cameras come with and expose a large number of camera parameters that directly affect the quality of the video stream capture. (2) While a few of such parameters, *e.g.,* exposure, focus, white balance are automatically adjusted by the camera internally, the remaining camera parameters are not. We denote such camera parameters as *non-automated (NAUTO) parameters*.

In this paper, we first show that as the environmental conditions around the cameras change, the quality of video frames captured by the cameras also changes, and this can adversely affect the accuracy of insights derived by the analytics units. In our experiments, we kept all automatic parameter setting features turned on and thus our experiments show that those automatic settings are not enough to adapt to different environments for better analytics accuracy.

Next, we experimentally show that by (manually) dynamically adjusting a prominent set of NAUTO camera parameters, in particular, four image appearance parameters including brightness, contrast, color-saturation (also known as colorfulness), and sharpness, which are available in both pan-tilt-zoom (PTZ) and non-PTZ cameras, it is possible to mitigate the potential loss in accuracy due to adverse environmental changes. We chose these NAUTO parameters in our study because they not only directly affect image qualities and hence AU accuracy but also are challenging to tune due to their large ranges of values.

Since streaming video analytics systems operate around the clock (24 hours a day, seven days a week), it is not practical for humans to manually adjust tens of configurable camera parameters in real-time in response to every environmental change. Therefore, we propose CAMTUNER, a system that detects and dynamically adapts to the changes in environmental conditions by automatically adjusting camera parameters in real-time to improve AU accuracy. CAMTUNER uses online reinforcement learning (RL) [48] to continuously learn good camera settings and update the camera parameters to enhance the accuracy of the AUs in the VAP. In particular, CAMTUNER uses SARSA [52], which is faster to train and achieves slightly better accuracy in our video stream processing context than other popular RL approaches like Q-learning.

Although RL is a fairly standard technique, applying it to tuning camera parameters in a real-time video analytics system poses two unique challenges.

First, implementing online RL requires knowing the reward/penalty for every action taken during exploration and exploitation. Since no ground truth for an AU task like face detection is available during the online operation of a VAP, calculating the reward/penalty due to an action taken by an RL agent is a key challenge. To address this challenge, we propose an *AU-specific analytics quality estimator* that can accurately estimate the accuracy of the AU. Our estimator is light-weight, and it can run on a low-end PC or a simple IoT device to process video streams in real-time.

Second, bespoke online RL learning at each camera deployment setup requires initial *RL training*, which can potentially take a long time for two reasons: (1) capturing the environmental condition changes such as the time-of-the-day effect can take a long time, and (2) taking an action on the real camera (*i.e.,* changing the camera parameter setting) by using the APIs provided by the camera vendor incurs a significant delay of about 200 ms. This limits the speed of state transitions during RL exploration, and hence the training speed of RL, to about 5 changes (actions) per second. To address these two sources of RL training inefficiencies, we propose a novel concept called *virtual camera*. A virtual camera mimics (in software) the effect of changing parameters of a physical camera to capture a scene. There are two key benefits of doing this: (1) we can complete an action of "camera setting change" almost instantaneously; and (2) we can digitally *augment* a single frame captured by the real camera to derive many new synthetically transformed frames, as if we had physically captured many different frames of the same scene by using a real camera at different environmental conditions (*i.e.,* time-of-day, lighting conditions, seasonal changes *etc.*). These two benefits allow the RL agent to explore actions at a much faster rate than possible in using a real camera. This drastically reduces the RL training time required to develop a good, initial RL model, which can then be further refined in a short period (adaptation phase) after camera deployment.

Our paper makes the following contributions:

- We show that environmental condition changes can have a significant negative impact on the accuracy of AUs in video analytics pipelines, but the negative impact can be mitigated by dynamically adjusting a set of NAUTO camera parameters.

- We develop, to our knowledge, the first system that automatically and adaptively learns and tunes the set of NAUTO camera parameters in response to unpredictable environmental condition changes to improve the accuracy of insights from video analytics pipelines.
- We present two novel techniques that make the RL-based camera-parameter-tuning design feasible: a light-weight AU-specific analytics quality estimator that enables online RL without requiring ground truth, and a virtual camera that enables fast initial RL model training.
- We show that CAMTUNER improves AU accuracy in controlled experiments and in real VAP deployment. In particular, in a real world deployment where two cameras deployed side-by-side (one camera is managed by CAMTUNER, while the other is not) are monitoring a large enterprise parking lot, and the live video streams are carried over a 5G network, the camera managed by CAMTUNER detected 15.9% (146) additional persons (in a 5-minute span) during evening hours, without any false positives. The camera managed by CAMTUNER detected 2.6%–4.2% (861–881) additional cars (in a 5-minute span) during morning and evening hours, again without any false positives.
- Furthermore, by recording a real-world car accident scenario at a traffic intersection (at one of our customer locations) and by using VC to emulate frame captures at different times of the day, the VAP with CAMTUNER reliably detected 9.7% (122) additional cars (across the frames in a 1.5-minute span), which dramatically improves the accuracy (and lead time) of collision prediction.
- We show that CAMTUNER incurs very low computation overhead and CAMTUNER can be easily incorporated into VAPs that are executing on low-end PC or IoT devices that are directly attached to the camera.

II. BACKGROUND

Figure 1 also shows the image signal processing (ISP) pipeline within a camera. Photons from the external world reach the image sensor through an optical lens. The image sensor uses a Bayer filter [6] to create raw-image data, which is further enhanced by a variety of image processing techniques such as demosaicing, denoising, white balance, color-correction, sharpening and image compression (JPEG/PNG or video compression using H.264 [5], VP9 [4], MJPEG, *etc.*) in the image-signal processing (ISP) stage [46] before the camera outputs an image or a video frame.

The camera capture forms the initial stage of the VAP, which may include a wide variety of analytics tasks such as face detection, face recognition, human pose estimation, license plate recognition *etc.* (see Figure 1).

In this paper, we study video analytics applications that are based on surveillance cameras. Such cameras are running 24X7 in contrast to DSLR, point-and-shoot or mobile cameras that capture videos on-demand. Popular IP video surveillance cameras are manufactured by vendors such as AXIS [16], Cisco [12], and Panasonic [25]. These surveillance camera manufacturers have exposed many camera parameters via REST APIs which can be set by applications to control the image generation process, which in turn affects the quality of the produced image or video. The exposed parameters include those for changing the amount of light that hits the sensor, the zoom level and field-of-view (FoV) at the image-sensor stage, and those for changing the color-saturation, brightness, contrast, sharpness, gamma, acutance, *etc.* in the ISP stage. Table I lists the parameters exposed by a few popular surveillance cameras in the market today. Remotely changing the camera setting via the exposed APIs, however, incurs a significant delay, *e.g.,* about 200 ms on Axis Q1615, Axis Q3515, Axis Q6128-E and Axis Q3505 MK II network camera.

TABLE I: Parameters exposed by popular cameras. Parameters with "*" are auto-adjusted by the camera internally.

Camera Setting Parameters		Video Stream Parameters	
Image Appearance	Brightness sharpness contrast color level	Image Appearance	Resolution Compression Rotate image
Exposure Settings	Exposure Control* Max Exposure Time Exposure Zones* Max gain IR cut filter*	Encoder Settings	GOP length H.264 profile
Image Correction	Defog Effect Noise Reduction Stabilizer Auto Focus Enabled*	Bitrate Control	Type of Use Target Bitrate Priority
White Balance	Type* window*	Video Stream	Max FPS
		MJPEG	Max frame size

While a few of these camera parameters, *e.g.,* exposure, focus, balance, are automatically adjusted by the camera internally, the remaining camera parameters are not adjusted automatically. We denote such camera parameters as *non-automated (NAUTO) parameters*.

In this paper, we focus our study on the four image appearance camera parameters, denoted as *I-A parameters* in the rest of the paper, which are widely available in both PTZ and non-PTZ cameras: *brightness, contrast, color-saturation* (also known as colorfulness), and *sharpness*. We choose the above four NAUTO camera parameters in our study in this paper for two reasons: (1) they directly affect the quality of the image which is essential to AUs which typically extract insights, *e.g.,* face recognition, from individual frames; (2) These parameters are more challenging to tune due to the large range (for example, between 1 and 100 for each of the parameters on Axis Q1615, Axis Q3515, Axis Q6128-E, Axis Q3505 MK II network camera *etc.*) compared to other NAUTO camera parameters which have either a few fixed settings or just a binary ON/OFF switch. Several AUTO parameters, *e.g.,* exposure and white-balance, affect the raw capture before the four I-A parameters are applied in the ISP stage. Thus, there is no mutual interference between those AUTO and I-A parameters when analyzing the impact of I-A parameters on capture quality.

III. MOTIVATION

We motivate the need for dynamically adjusting NAUTO camera settings by experimentally showing the impact of environmental changes on AU accuracy despite all the auto-setting features are left on, and that tuning a set of NAUTO

This article has been accepted for publication in IEEE Transactions on Mobile Computing. This is the author's version which has not been fully edited and content may change prior to final publication. Citation information: DOI 10.1109/TMC.2025.3540667

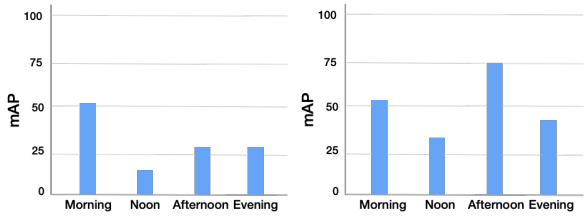

(a) Face detection (b) Person detection

Fig. 3: AU accuracy variation in a day under the default camera setting.

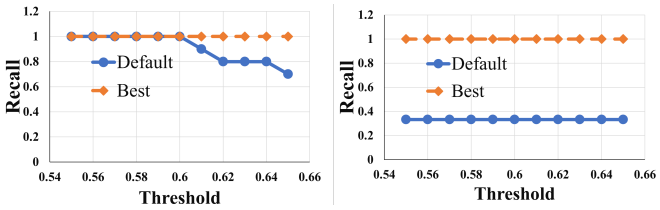

(a) DAY (b) NIGHT

Fig. 4: Impact of parameter tuning impact on Face-recognition.

camera settings can improve AU accuracy under the same environmental conditions.

A. Impact of Environment Change on AU Accuracy

Environmental changes happen for at least three reasons. First, such changes can be induced due to the change of the Sun's movement throughout a day, *e.g.,* sunrise and sunset. Second, they can be triggered by changes in weather conditions, *e.g.,* rain, fog, and snow. Third, even for the same weather condition at exactly the same time of the day, the videos captured by the cameras at different deployment sites (*e.g.,* parking lot, factory, shopping mall, and airport) can have diverse content and ambient lighting conditions.

To illustrate the impact of environmental changes on image quality, and consequently on the accuracy of AUs, we experimentally measure the accuracy of two popular AUs (face detection and person detection) throughout a 24-hour (one-day) period. Since there are no publicly available video datasets that capture the environmental variations in a day or a week by using the same camera (outside the baseball stadium which was fairly crowded throughout the day), we use several proprietary videos provided by our customers that were captured with the default camera setting – in this paper, *the default camera setting* refers to when all auto-setting features are turned on and NAUTO parameters are set to the default values provided by the manufacturers. These videos were captured outside airports and baseball stadiums by stationary surveillance cameras, and we have labeled ground-truth information for several analytics tasks including face detection and person detection.

We use RetinaNet [18] for face detection and EfficientDet-v8 [50] for person detection. We compute the mean Average Precision (mAP) by using pycocotools [15]. Figure 3a shows that the average mAP values for the face detection AU during four different time periods of the day (morning 8AM - 10AM, noon 12PM - 2PM, afternoon 3PM - 5PM, and evening 6PM - 8PM), and with the default camera setting, can vary by up to 40% as the day progresses (blue bars). Similarly, Figure 3b shows that the average mAP values for the person detection AU (with the default camera parameter setting) can vary by up to 38% during the four time periods. We also observed similar accuracy variation while using other face-detection (MTCNN) and person-detection models (Yolov5). These results show that changes in environmental conditions can adversely affect the quality of the frames retrieved from the camera, and consequently adversely impact the accuracy of the insights that are derived from the video data.

B. Impact of Image Appearance Camera Settings on AU Accuracy

We experimentally show that adjusting the four image appearance (I-A) (NAUTO) camera settings, *i.e.,* brightness, contrast, color-saturation (also known as colorfulness), and *sharpness*, can help to mitigate the adverse impact of environmental changes on AU accuracy.

Analyzing the impact of camera settings on video analytics in general faces a significant challenge: it requires applying different camera parameter settings to the same input scene and measuring the resulting accuracy of insights from an AU. The straightforward approach is to use multiple cameras with different camera parameter settings to capture the same input scene. However, this approach is impractical as there are thousands of different combinations of even just the four camera parameters we consider. To overcome the challenge, we proceed with the following workaround which uses a single real camera.

Face-recognition VAP on static images: In this experiment, we place face cutouts of 10 unique individuals in front of the camera as a fixed static scene and evaluate the performance of the most accurate face-recognition AU, Neoface-v3 [42][1], for various camera settings and for different face matching thresholds. Since this face-recognition AU has high precision despite environmental changes, we focus on measuring Recall, *i.e.,* true-positive rate. Here, we use a real camera, Axis Q3505 MK II Network camera.

We rerun this experiment for two environmental conditions, *i.e.,*DAY and NIGHT conditions in our lab, simulated using two sources of light. One of them is always kept *ON*, while the other light source is manually turned ON or OFF to simulate DAY and NIGHT environmental conditions, respectively.

We compare AU results under the manufacturer-provided "Default" camera settings and "Best" settings for the four camera parameters. To find the "Best" settings, we exhaustively change the four camera parameters to find the setting that gives the highest Recall value. Specifically, we vary each parameter from 0 to 100 in steps of 10 and capture the frame for each camera setting. This gives us ≈14.6K (11^4) frames for each condition. Changing one camera setting through the VAPIX API takes about 200ms, and in total it took about *7 hours* to capture and process the frames for each condition.

Figure 4a shows the Recall for the DAY condition for various thresholds. Figure 4b shows the recall for the night condition

[1]This face-recognition AU is ranked first in the world in the most recent face-recognition technology benchmarking by NIST.

This article has been accepted for publication in IEEE Transactions on Mobile Computing. This is the author's version which has not been fully edited and content may change prior to final publication. Citation information: DOI 10.1109/TMC.2025.3540667

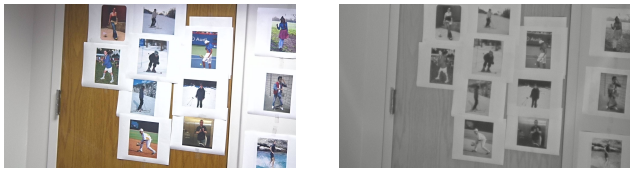

(a) DAY (b) NIGHT

Fig. 5: Camera captures under different environments.

for various thresholds. We see that (1) under the "default" setting, the recall for the day condition goes down at higher thresholds, indicating that some faces were not recognized, whereas for the night condition, the recall remains constant at a low value for all thresholds, indicating that some faces were not being recognized regardless of the face matching thresholds. (2) in contrast, when we changed the camera parameters for both conditions to the "Best" settings, the AU achieves the highest Recall (100%), confirming that all the faces are correctly recognized. (3) The "Best" settings for DAY condition ([80,80,60,40]) is different from that for NIGHT condition ([100,90,30,70]). In the appendix, we illustrate the performance variations of an object detection VAP in a real-world video scene and discuss the optimal adjustment of camera parameters in response to environmental changes.

C. Optimal camera setting is AU-specific

Along with the environment, to observe the impact of camera parameters on various AUs, we printed 12 different person cutouts obtained from COCO dataset [35] and placed them in front of an Axis network camera. we use Efficientdet [50] as person-detection AU and RetinaNet [18] as face-detection AU and observe the impact on each of these AUs individually under *DAY* and *NIGHT* condition simulated inside our lab using two light sources. One of them is always kept *ON*, while the other light source is manually turned ON or OFF to simulate DAY and NIGHT environmental conditions, respectively. For each of these conditions, we vary the four image appearance camera parameters, *i.e.,* brightness, contrast, sharpness and color-saturation ranging from 0 to 100 at a step of 10. Figure 5 shows the images captured under the default camera setting for *DAY* and *NIGHT* condition. To find the "Best" settings for a specific AU, we change the four camera parameters to find the setting that gives the *highest mAP*. Specifically, we vary each parameter from 0 to 100 in steps of 10 and capture the frame for each camera setting. This gives us ≈14.6K (11^4) frames for each condition. Changing the camera setting through the VAPIX API takes about 200ms, and in total it took about *7 hours* to capture and process the frames for each condition.

Table II shows that the best I-A camera parameter setting for different AUs are unique. Furthermore, these *Best* camera settings not only vary across different AUs but change due to environmental condition changes (i.e., from DAY to NIGHT), also shown in Table II. This motivates the need for capturing AU specific perception in tuning the camera parameters.

IV. Design Challenges

Designing CamTuner to automatically tune camera parameter settings to enhance video analytics accuracy faces several challenges. In this section, we discuss these challenges and our approaches to address each one of them.

TABLE II: Best settings across different AUs for various env.

AU-best	Best camera setting [brightness, contrast, color, sharpness]	
	DAY	NIGHT
Person Detection-best	[80,90,70,100]	[40,90,60,100]
Face Detection-best	[80,90,60,80]	[60,40,90,90]

Challenge 1: Identifying the best camera setting for a particular scene. Cameras deployed across different locations observe different scenes. Moreover, the scene observed by a particular camera at any one location keeps changing based on the environmental conditions, lighting conditions, movement of objects in the field of view, etc. In such a dynamic environment, how can we identify the best camera setting that will give the highest AU accuracy for a particular scene? The straightforward approach of collecting data for all possible scenes that can ever be observed by the camera and training a model that gives the best camera settings for a given scene is infeasible.

Challenge 2: No Ground truth in real-time. Implementing online RL requires knowing the reward/penalty for every action taken during exploration and exploitation, *i.e.,* what effect a particular camera parameter setting will have on the accuracy change of the AU. Since no ground truth of the AU task, *e.g.,* face detection, is available during normal operation of the real-time video analytics system, detecting a change in accuracy of the AU during runtime is challenging.

Challenge 3: Extremely slow initial RL training. Online learning at each camera deployment setup requires initial RL training, which can potentially take a very long time for two key reasons: (1) Capturing the environmental condition changes such as the time-of-the-day effect requires waiting for the Sun's movement through the entire day until night, and capturing weather changes requires waiting for weather changes to actually happen. (2) Taking an action on the real camera, *i.e.,* changing the camera parameter setting, incurs a significant delay of about 200 ms. This delay fundamentally limits the speed of state transition and hence the learning speed of RL to only 5 actions per second.

V. $CamTuner$ Design

Figure 6 shows the system-level architecture for CamTuner, which automatically and dynamically tunes the camera parameters to enhance the accuracy of AUs in the VAP. CamTuner augments a standard VAP shown in Figure 1 with two key components: a Reinforcement Learning (RL) engine, and an AU-specific analytics quality estimator. In addition, it employs a third component, a Virtual Camera (VC), for fast initial RL training.

A. Reinforcement Learning (RL) Engine

The RL engine is the heart of CamTuner system, as it is the one that automatically chooses the best camera settings for a particular scene. Q-learning [51] and SARSA [52] are two popular RL algorithms that are quite effective in learning the best action to take in order to maximize the reward. We compared these two algorithms and found that training with SARSA achieves slightly faster convergence and also slightly

This article has been accepted for publication in IEEE Transactions on Mobile Computing. This is the author's version which has not been fully edited and content may change prior to final publication. Citation information: DOI 10.1109/TMC.2025.3540667

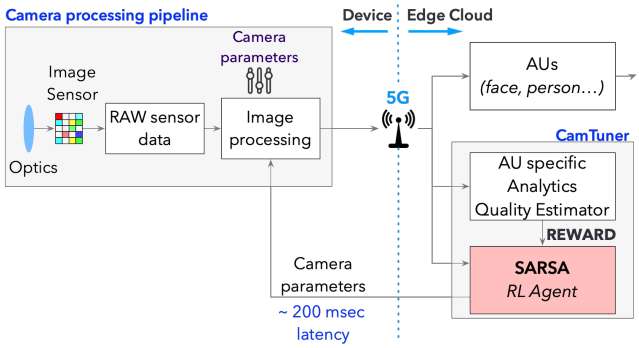

Fig. 6: $CamTuner$ system design. $CamTuner$ augments a standard VAP shown in Figure 1 with two key components: a Reinforcement Learning (RL) engine, and an AU-specific analytics quality estimator.

Algorithm 1: State-Action-Reward-State-Action loop.

```
s ← Observe-Environment()
// ϵ-greedy policy to select next action
a ← Choose-Action(Q, s, ϵ)
while Still-Processing() do
    Perform-Action(a)
    r ← Compute-Reward()
    s' ← Observe-Environment()
    a' ← Choose-Action(Q, s', ϵ)
    Q(s, a) ← Q(s,a) + α × [r + γ × Q(s', a') – Q(s, a)]
    s ← s'
    a ← a'
end
```

better accuracy than with Q-learning. Therefore, we use SARSA RL algorithm in CAMTUNER.

SARSA is similar to other RL algorithms. The steps followed by an SARSA RL agent are shown in Algorithm 1. Here, the agent first observes the environment, *i.e.,* state s, and chooses an appropriate action a to be performed in state s. After performing the action a, the agent receives an immediate reward (or penalty) r and is now in a new state s'. In this new state, the action chosen by the agent is a' and the associated Q-value is $Q(s', a')$, which the agent uses to compute the cumulative reward $Q(s, a)$ as per equation 1. The agent then updates this computed cumulative Q-value and is now in the new state s'. This process continues for the lifetime of the AU as the agent continuously learns and adapts to the environment.

SARSA does not require any labeled data or pre-trained model, but it does require a clear definition of the *state*, *action* and *reward* for the RL agent. This combination of *state*, *action* and *reward* is unique for each application and needs to be carefully chosen, so that the agent learns exactly what is desired. In our setup, we define them as follows:

State: A state is a tuple of two vectors, $s_t =< P_t, M_t >$, where P_t consists of the current brightness, contrast, sharpness, and color-saturation parameter values on the camera, and M_t consists of the measured values of brightness, contrast, color-saturation, and sharpness of the captured frame at time t, measured as in [7], [44], [23], [17].

Action: The set of actions that the agent can take are (a) increasing or decreasing one of the brightness, contrast, sharpness or color-saturation parameter value, or (b) not changing any parameter values. We choose the increase or decrease of camera parameters at a granularity of 10 only. The choice of such a granularity of camera parameter setting adjustment is to strike a balance between adjustment complexity and potential gain. In particular, we search in a discrete action space of increments of 10 to make the camera parameter tuning problem tractable.

Reward: We use an AU-specific analytics quality estimator as the immediate reward function (r) for the SARSA algorithm. Along with considering immediate reward, the agent also factors in future reward that may accrue as a result of the current actions. Based on this, a value, termed as Q-value (also denoted as $Q(s_t, a_t)$) is calculated for taking an action a_t when in state s_t using Equation 1.

$$Q(s_t, a_t) \leftarrow Q(s_t, a_t) + \alpha\left[r + \gamma \cdot Q(s_{t+1}, a_{t+1}) - Q(s_t, a_t)\right] \quad (1)$$

Here, α is learning rate (a constant between 0 and 1) used to control how much importance is to be given to new information obtained by the agent. A value of 1 will give high importance to the new information while a value of 0 will stop the learning phase for the agent.

Similar to α, γ (also known as the discount factor) is another constant used to control the importance given by the agent to any long term rewards. A value of 1 will give very high importance to long term rewards while a value of 0 will make the agent ignore any long term rewards and focus only on the immediate rewards. If the environmental conditions change very frequently, a lower value, *e.g.,* 0.1, can be assigned to γ to prioritize immediate rewards, while if the conditions do not change frequently, a higher value, *e.g.,* 0.9, can be assigned to prioritize long term rewards.

Exploration vs. Exploitation. We define a constant called ϵ (between 0 and 1) to control the balance between exploration vs. exploitation in taking actions. At each step, the agent generates a random number between 0 and 1; if the random number is greater than the set value of ϵ, then a random action (exploration) is chosen.

B. AU-specific Analytics Quality Estimator

In online operations, the RL engine needs to know whether its actions are changing the AU accuracy in the positive or negative direction. In the absence of ground truth, the *analytics quality estimator* acts as a guide and generates the reward/penalty for the RL agent.

Challenges. There are three key challenges in designing an online analytics quality estimator. **(1)** During runtime, AU quality estimation has to be done quickly, which implies a model that is small in size. **(2)** A small model size implies using a shallow neural network. For such a network, what representative features should the estimator extract that will have the most impact on the accuracy of AU output? **(3)** Since different types of AUs (*e.g.,* face detector, person

This article has been accepted for publication in IEEE Transactions on Mobile Computing. This is the author's version which has not been fully edited and content may change prior to final publication. Citation information: DOI 10.1109/TMC.2025.3540667

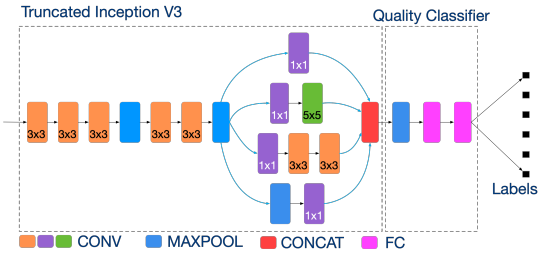

Fig. 7: AU-specific analytics quality estimator design.

detector) perceive the same representative features differently, the estimator needs to be AU-specific.

Insights. We make the following observations about estimating the quality of AUs. **(1)** Though estimating the precise accuracy of AU on a frame requires a deep neural network, estimating the coarse-grained accuracy, *e.g.,* in increments of 1%, may only require a shallow neural network. This insight is based on the observation that binning the accuracy into coarse-grained bins (with 1% increments) and predicting which bin the accuracy of the DNN falls into is a simpler task than estimating the precise accuracy. **(2)** Most of the "off-the-shelf" AUs use convolution and pooling layers to extract representative local features [10]. In particular, the first few layers in the AUs extract low-level features such as edges, shapes, or stretched patterns that affect the accuracy of the AU results. We can reuse the first few layers of these AUs in our estimator to capture the low-level features. **(3)** To capture different AU perceptions from the same representative features extracted in the early layers, we need to design and train the last few layers of each quality estimator to be AU-specific. During training, we need to use AU-specific quality labels.

Design. Motivated by the above insights, we design our light-weight AU-specific analytical quality estimator to consist of two components: (1) feature extractor and (2) quality classifier, as shown in Figure 7. We use supervised learning to train the AU-specific quality estimator.

Feature Extractor. Different AUs and environmental conditions can manipulate local features of an input frame at different granularities [22]. For example, blur (*i.e.,* motion or defocus blur) affects fine textures while light exposure affects coarse textures. While face detector and face recognition AUs focus on finer face details, person detector is coarse-grained and it only detects the bounding box of a person. Similarly, in convolution layers, larger filter sizes focus on global features while stacked convolution layers extract fine-grained features. To accommodate such diverse notions of granularities, we use the Inception module from the Inception-v3 network [49], which has convolution layers with diverse filter sizes.

Quality classifier. The goal of the quality classifier is to take the features extracted by the feature extractor and estimate the coarse-grained accuracy of the AU on an input frame, *e.g.,* in increments of 1%. As such, we divide the AU-specific accuracy measure into multiple coarse-grained labels, *e.g.,* from 0% to 99%, and use fully-connected layers whose output nodes generate AU-specific classification labels.

Detailed design and training of two concrete AU-specific analytics quality estimators are described as follows.

(1) Face recognition AU: The quality classifier of face recognition consists of 2 fully-connected layer and has 101 output classes. One of the classes signifies no match, while the remaining 100 classes correspond to match scores between 0 to 100% in units of 1%.

To generate the labeled data, we used 300 randomly-sampled celebrities from the celebA dataset [37]. We choose two images per person. We use one of them as a reference image and add it to the gallery. We use the other image to generate multiple variants by applying digital transformations on the image. These variants (∼4 million) form the query images. For each query image, we obtain the match score (a value between 0 and 100%) using the Face recognition AU, *Neoface-v3*. The query images along with their match score form the labeled samples, which are used to train the quality estimator.

(2) Face and object detection AU. The quality classifier of face and object (*i.e.,* car and person) detection AU consists of 2 fully-connected layers, and has 201 output classes to predict the quality estimate of the face and object detection AU for a given frame. One of the classes signifies AU cannot detect anything accurately, and the remaining 200 classes correspond to the cumulative mAP score between 0 to 100 and IoU score between 0 to 1, *i.e.,* $mAP + IOU_{True-Positive} * 100$. To generate the labeled data to train face-detection AU specific quality estimator, we used the Olympics [39] and HMDB [33] datasets, and created ∼7.5 million variants of the video frames by applying digital transformations. Then, for each frame, we use the face detection AU (*i.e.,* RetinaNet [18]) to determine the analytical quality estimate. Similarly, we use the object detection AU (*i.e.,* EfficientDet [50]) on labeled images from COCO dataset [35] that contain car and person object classes and their augmented variants. The video frames/images and their quality estimates form the labeled samples, which are used to train the estimator model.

For both the classifier training, we use a cross-entropy loss function to train AU-specific analytics quality estimators, initial learning rate is 10^{-5}, and we use Adam Optimizer [31]

C. Virtual Camera

We design a virtual camera (VC) to accelerate initial RL training by mimicking the effect of environmental conditions and camera setting changes on the frame capture of a real camera. In particular, the VC can takes a frame captures at one time of the day t_1 and renders it for a different time of the day t_2 as if it was captured by the camera at time t_2.

Motivation for VC. The Virtual Camera (VC) provides significant flexibility for training and evaluating CamTuner. Given that environmental conditions change very slowly, training (or exploring) an RL agent to learn diverse conditions throughout the day can be time-consuming if we wait for the conditions to change naturally, *e.g.,* which generates only one set of data per day. To address this, we utilize a Virtual Camera (VC) that can render the same frame at different capture times of the day. In its current version, the VC augments frames by adjusting brightness, color, contrast, and sharpness to simulate various times of the day. We plan to enhance the VC with adjusting additional settings in future iterations.

More specifically, the VC can enhances the CamTuner design in several ways:

This article has been accepted for publication in IEEE Transactions on Mobile Computing. This is the author's version which has not been fully edited and content may change prior to final publication. Citation information: DOI 10.1109/TMC.2025.3540667

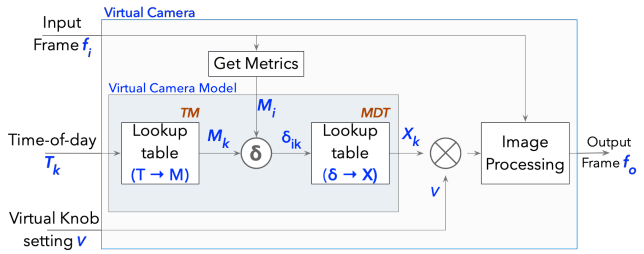

Fig. 8: VC block diagram.

Time-of-day (T_k)	Metric Tuple (M_k)		
	tile_1	tile_2	.....
10:00	<159,53,1 1,2122>	<157,55,9, 2103>	.....
10:15	<160,52,1 3,2100>	<159,56,1 5,2080>	.....
.....	.....	.....	.....

(a) TM table

Delta Change (δ)	Transformation Tuple (X)
<0.5,0.7,1.5,2>	<0.7,0.6,1.1,1.2>
<10,18,5,9>	<1.5,2.4,1.6,1.5>
.....	.....

(b) MDT Table

Fig. 9: Offline generated tables for VC.

1) *Experimental control and reproducibility*: The VC allows us to apply various camera parameter configurations to the exact same scene, ensuring repeatability and reproducibility in our experiments, which is not feasible with a real camera.
2) *Faster experimentation*: Unlike a real camera which captures at 25-30 frames per second, the VC can process video frames at much higher speeds, up to 300 frames per second, significantly accelerating experimentation.
3) *Independent testing and training*: The VC enables independent testing and training of RL algorithms with various reward functions.

Additionally, in scenarios where multiple Analytics Units (AUs) operate on a single video feed, each AU might require different optimal camera settings. A real camera can only apply one camera setting at any given time, but the VC can simulate custom "best" settings for each AU according to its specific requirements.

Definition. A VC (shown in Figure 8) takes an input frame f_i, captured by a real camera, the target time-of-the-day T_k, and VC parameter settings V, as input, and outputs a frame f_o as if it was captured by the physical camera at time T_k. To generate a frame at time T_k, VC uses a composition function $Compose(X_k, V)$, which composes output frame f_o using X_k, which is the transformation that augments the environmental effects corresponding to the target time T_k on input frame f_i, and V, which is the VC parameter settings. The composition function is defined as $X_k * 10^{V-0.5}$, which considers X_k and V simultaneously, similar to a real camera. Using this composition function, X_k is scaled up if the value of V is greater than 0.5 and scaled down if the value is less than 0.5; no scaling of X_k happens for V equal to 0.5.

To understand how VC works, we first introduce an important definition. Each frame f_i, from a real physical camera, possesses distinct values of brightness, contrast, colorfulness and sharpness metrics, denoted as a *metric (or feature) tuple* $M_i =< \alpha_M, \beta_M, \gamma_M, \zeta_M >$. The unique metric tuple encapsulates the environmental conditions and the default physical camera settings when the frame was captured.

Offline profiling phase: VC derives two tables for a given physical camera deployment during an offline profiling phase and then uses the two tables during online operation to generate the output frame f_o.

The first table (TM) maps a given time-of-the-day T_k to the metric tuple M_k which captures the distinct values of brightness, contrast, colorfulness and sharpness metrics of frames taken by the physical camera with the default settings at time T_k. Since, metric tuples for different part of the frames show different profiles as shown in Figure 10, we generate the table to cover the full 24-hour period with a granularity of 15 minutes, *i.e.,* the table has one mapping for every 15 minutes, for a total of 96 mappings. To construct the table, we use a full 24-hour long video and break it into 15-minute video snippets. We extract all the frames from the video snippet for each 15-minute interval T_k. , we divide each frame into 12 tiles as shown in Figure 11 , obtain the corresponding metric tuple for each tile, and compute the mean metric tuple for the corresponding tiles in all frames in the 15-minute interval as the metric tuple for that tile, and the list of tuples for all 12 tiles form the entry for time T_k in the table, as shown in Figure 9a.

The second table (MDT) maps the difference between two metric tuples M_i and M_k, $\delta(M_i, M_k)$, to the corresponding transformation tuple X_k that would effectively transform a frame captured by the physical camera with metric tuple M_i to become a frame captured by the physical camera for the same scene with metric tuple M_k. We note since each camera parameter can take 11 values, from 0 to 100 with increments of 10, the difference between any two metric tuples can possibly be mapped to one of these 14K (11^4) settings. We construct the entries for the table backward as follows. (1) We select a random frame from each 15-minute interval to form a collection of 96 frames with varying environmental conditions, *i.e.,* corresponding to different time-of-the-day. (2) For each possible transformation X_k, we transform the 96 frames into 96 virtual frames. We then obtain the delta metric tuples between each pair of original and transformed frames, calculate the median of the 96 delta metric tuples, δ_k, and store the pair of $< \delta_k, X_k >$ in the table. (3) We repeat the above process for all possible transformation settings (14K in total) to populate the table, as shown in Figure 9b.

Finally, at runtime when the table is used by the VC, if the entry for a given delta metric tuple δ_i is empty, we return the entry whose delta metric tuple δ_k is closest to δ_i using L1-norm.

Online phase. VC transforms the input frame f_i to output frame f_o in five steps. (1) It measures the current metric tuple $M_i =< \alpha_M, \beta_M, \gamma_M, \zeta_M >_{curr}$ from input frame f_i; (2) It looks up *Time-to-Metric (TM)* table for the metric tuple $M_k =< \alpha_M, \beta_M, \gamma_M, \zeta_M >_{desired}$ that corresponds to the target time of the day (T_k); (3) It calculates the difference between M_i and M_k, $\delta(M_i, M_k)$ or δ_{ik}; (4) It looks up *Metric-difference-to-Transformation (MDT)* table to find the transformation $X_k =< \alpha_X, \beta_X, \gamma_X, \zeta_X >_{applied}$ that corresponds to δ_{ik}; (5) It applies X_k along with V using the composition function $Compose(X_k, V)$ to input frame f_i and

This article has been accepted for publication in IEEE Transactions on Mobile Computing. This is the author's version which has not been fully edited and content may change prior to final publication. Citation information: DOI 10.1109/TMC.2025.3540667

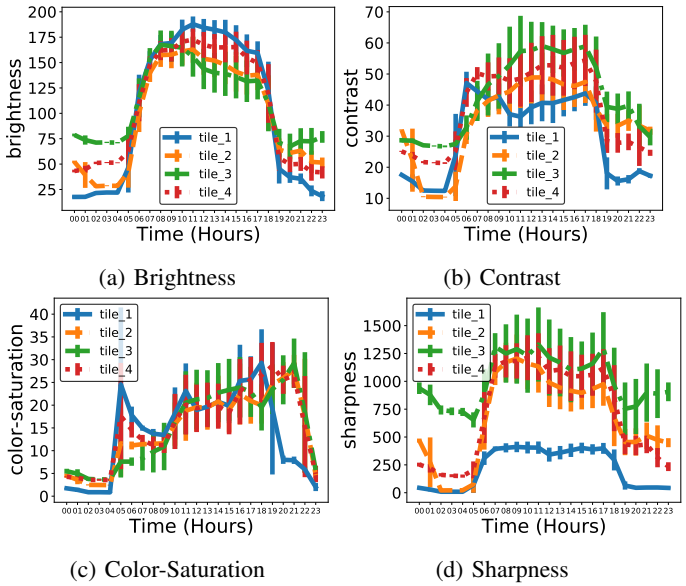

(a) Brightness (b) Contrast

(c) Color-Saturation (d) Sharpness

Fig. 10: Day-long feature profiles for different tiles.

Fig. 11: Tiled representation of a captured frame.

generates output frame f_o.

Since different parts of an input frame may exhibit varying local feature or metric values, to improve the effectiveness of virtual knob transformation, instead of applying the above steps directly to input frame f_i, we split it into 12 (3 X 4) equal-sized tiles, as shown in Figure 11, apply Steps 1-3 to each of the 12 tiles, *i.e.,* each of M_i, M_k, and δ_{ik} consists of 12 sub-tuples corresponding to the 12 tiles, respectively. The 12 sub-tuples in δ_{ik} are looked up in the MDT table to find 12 transformation tuples. Finally, to ensure smoothness, we calculate the mean of these 12 sub-tuples X_k, which is then applied to input frame f_i.

D. Integrating VC with the RL engine

During initial RL training, the RL agent performs *fast exploration* by leveraging VC as follows. It reads each frame f_i from the input training video, and repeats the following exploration steps for all time-of-the-day values T_k. At each exploration step j, the agent which is at state $s =< P_j, M_j >$ performs tasks: (1) based on current state (s), it takes a random action a and apply that on V_j, which is VC equivalent of P_j for a real camera, to get a new virtual knob setting for next exploration step $(j+1)$, V_{j+1}; (2) it invokes the VC with frame f_i for the target time-of-the-day T_k, and current VC parameters V_{j+1} as input, and the VC outputs frame f_o. The measured tuple M_{j+1} of brightness, contrast, colorfulness and sharpness metric values of output frame f_o along with the virtual knob setting V_{j+1}, form the new state of the RL agent, $s_{new} =< V_{j+1}, M_{j+1} >$; (3) it calculates the reward/penalty by feeding f_o into the AU-specific quality estimator; and (4) it updates the Q-table entry $Q(s, a)$.

The above initially trained SARSA model with the VC is then deployed in the real camera for the normal operations of CAMTUNER. First, the ϵ value is set to low (0.1) and α is set to high (0.85) so that the SARSA RL agent will go through a short *adaptation* phase, *e.g.,* for an hour, by performing primarily exploration. Afterward, the ϵ and α values are set to high (0.9) and low (0.15), respectively, so that SARSA performs primarily exploitation using the trained model. We use a γ of 0.9. We also use a smoothing parameter of 0.7 as the weight parameter of the exponential weighted average that is used to modify any Q-table entry.

VI. IMPLEMENTATION

A. Hardware Setup

For the evaluation, we implemented a VAP using an Axis Q3505 MK II network surveillance camera. We run CAMTUNER on a low-end Intel NUC box [2] while face detection and object detection AUs and initial pre-training with VC run on a high-end edge-server equipped with Xeon(R) W-2145 CPU and GeForce RTX 2080 GPU. The captured frames are sent for AU processing on the edge-server over a 5G network with an average frame uploading latency of 39.7 ms.

B. Software Implementation

We implemented the SARSA RL agent in Python, the light-weight AU-specific analytics quality estimators in pytorch framework which runs as a service using the ZeroMQ [3] networking library, and the Virtual Camera in Python which is trained on the GPU edge server. We use PIL [13] and OpenCV [2] for image processing during the offline profiling phase in VC design and also during offline training of the SARSA RL agent. We use Axis' *VAPIX* API to change the camera parameters decided by the SARSA-RL agent as well as to capture input frames.

Similar to a real camera, our VC runs continuously during offline SARSA RL training and streams the output frames on a NATS [1] queue at the same frames-per-second (FPS) with which the video was captured. Each frame is sent in BSON format which includes the frame number, frame data (*i.e.,* array of bytes), and timestamp. Like a real camera, VC exposes REST APIs that are used to query and change its settings to allow augmenting various environmental effects.

VII. EVALUATION

We extensively evaluate the effectiveness of CAMTUNER by measuring its impact on AU accuracy improvement in a VAP via controlled experimental emulation and in a real deployment (§VII-A – §VII-C). We also evaluate its system performance (§VII-D) and the efficacy of its two key components, AU-specific analytics quality estimator and VC (§VII-E).

[2]Currently it is performed at the edge (an Intel-NUC box), but camera parameter tuning can be performed either at the edge or on a device.

This article has been accepted for publication in IEEE Transactions on Mobile Computing. This is the author's version which has not been fully edited and content may change prior to final publication. Citation information: DOI 10.1109/TMC.2025.3540667

A. End-to-end VAP Performance

We first evaluate the effectiveness of CAMTUNER by comparing AU accuracy of five different VAPs.

1) Experimental Setup: We compare three CAMTUNER variants against two baseline VAPs. All system variants, including CAMTUNER, only differ in how the four I-A camera parameters are tuned, while keeping all automatic parameter setting features turned on and the rest NAUTO parameters at the default values. (1) *Baseline*: In the Baseline VAP, the I-A camera parameters are not adapted to any environmental changes. (2) *Strawman*: The Strawman approach applies a time-of-the-day heuristic that tunes the four I-A camera parameters based on a human perception metric. In particular, we use the BRISQUE quality metric [38] and exhaustively search for the best camera parameters for the first few frames in each hour and then apply the best camera setting found for the remaining frames in that hour. This exhaustive search of camera settings using initial frames takes a few minutes (which is expensive) and our results show that performing this adaptation more often than once per hour does not give significant improvement. (3) CAMTUNER-β: This variant of CAMTUNER only uses a few rounds of online exploration (*i.e.,* which takes about 1 hour, same as in online exploration performed by CAMTUNER), *i.e.,* the SARSA RL agent does not rely on the VC for initial offline exploration. Instead, at the start of online exploration, the CAMTUNER-β framework is initially seeded with an empty Q-table. (4) CAMTUNER-α: This variant of CAMTUNER adjusts the I-A camera setting dynamically by using only the offline trained SARSA RL agent, *i.e.,* the agent does not perform any exploration during online operation. (5) CAMTUNER: The complete CAMTUNER framework is seeded with offline trained SARSA RL agent, and then during online operation, the agent continues exploration initially and then moves towards exploitation, as described in §V-D. For CAMTUNER-β, CAMTUNER-α and CAMTUNER, the RL agent adaptively adjusts the four I-A camera parameters periodically; the time interval is configurable and we choose it to be *10s*.

Experimental methodology. Comparing these 5 VAPs in a real-world deployment is difficult because (1) even with 5 co-located cameras, it is difficult to see the identical scene from the same angle; (2) furthermore, in a real-world deployment, the captured scenes do not have the ground-truth to measure the AU accuracy. To overcome the above challenge, we loop a pre-recorded (original) 5-minute video snippet (a customer video captured at an airport) labeled with ground-truth through VC – VC is used here not for RL training but for generating *augmented* input videos that emulate different environmental changes to be fed into the five VAPs. In particular, we gradually change the VC model parameters (*i.e.,* digital transformations) to simulate the changes that happen during the day as the Sun changes its position and finally sets, and we ensure (through manual inspection) that same ground-truths are carried over in the VC generated videos from the original video. We then project these VC-generated videos on a monitor screen in front of a real camera, and run each of the five VAPs in turn. We note that the above controlled experimental setup is the closest approximation to a real-world deployment.

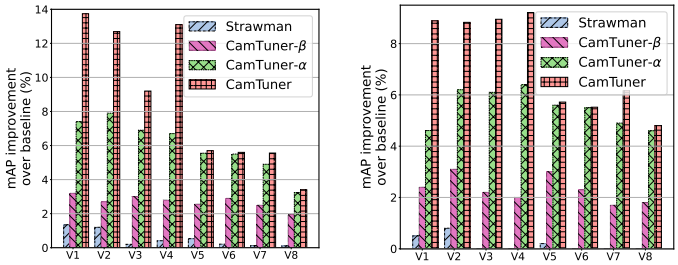

(a) Face detection AU (b) Person detection AU

Fig. 12: mAP improvements for different AUs.

2) End-to-end Accuracy: We evaluate the AU accuracy improvement of VAPs 2-5 over VAP 1 for eight 5-minute video segments randomly selected from the VC-generated videos consisting of 7500 frames each, and the video segments are separated by 1 hour apart. Using the labeled ground-truth, we evaluate the detection accuracy of the 5 VAPs for face-detection and person-detection AUs.

Figure 12 shows the bar-plot of mAP improvement of VAPs 2-5 over VAP 1 for the eight 5-min video segments corresponding to eight different hours of the day. We make the following observations. The strawman approach based on the *time-of-the-day* heuristic can provide only nominal improvement over Baseline, *i.e.,* less than 1% on average across the videos for both face detection and person detection. Just a few hours of "slow" online exploration (*i.e.,* with no VC-accelerated offline exploration) enables CAMTUNER-β to improve face detection accuracy by 2.70% on average and person detection accuracy by 2.31% on average over Baseline. In contrast, *fast* offline exploration using virtual camera (with no online exploration) helps CAMTUNER-α to improve face detection accuracy by 6.01% on average and person detection accuracy by 5.49% on average over Baseline. Finally, dynamically tuning the real camera parameters with online learning in CAMTUNER improves the face detection AU accuracy by up to 13.8% and person detection AU accuracy by up to 9.2%, with an average improvement of 8.63% and 8.11% for face detection AU, and average improvement of 7.25% and 7.08% for person detection AU compared to Baseline and Strawman, respectively. Note that the environment observed by the camera during the hours corresponding to bars v5-v8 in Figure 12 has not changed significantly while the environment observed for bars v1-v4 is largely different from that during offline exploration. This explains why the improvement gap between CAMTUNER-α and CAMTUNER over VAP 1 seems to diminish for bars v5-v8.

In summary, during offline phase VC helps the SARSA RL agent to quickly train through fast and equivalent environmental changes and camera parameter changes applied to the input scene. Then during online operation, a few rounds of exploration helps CAMTUNER to achieve better accuracy than directly using the initially trained SARSA model with VC (CAMTUNER-α).

3) In-depth Analysis: Next, we show how CAMTUNER dynamically adjusts the camera parameter setting for one of the 5-minute video snippet (*i.e.,* V3 in Figure 12) used in

This article has been accepted for publication in IEEE Transactions on Mobile Computing. This is the author's version which has not been fully edited and content may change prior to final publication. Citation information: DOI 10.1109/TMC.2025.3540667

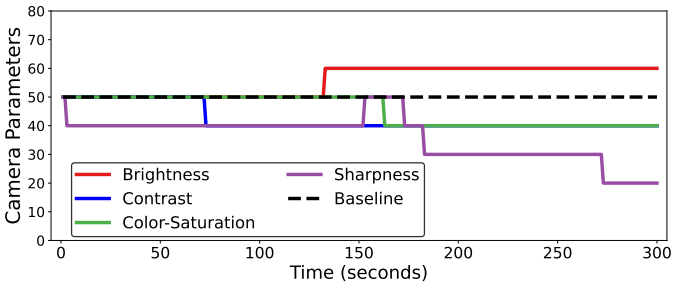

(a) Camera setting adaptation

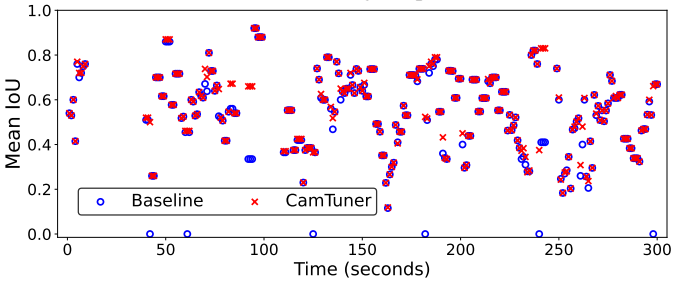

(b) mIoU variation

Fig. 13: *CamTuner* in operation during morning.

§VII-A2 for *face-detection AU*. Recall at every 10 seconds, based on the current environmental condition and content seen by the camera, CAMTUNER either chooses to "increment" or "decrement" one of the four parameters, *i.e.,* increase or decrease by 10 within the parameter range of [0, 100], or keep the previous parameter setting. Figure 13a shows how the camera parameters are adapted throughout the video length during the exploitation phase, and Figure 13b shows how the corresponding mean intersection-over-union (mIoU) (*i.e.,* IoU across all ground-truth bounding boxes in each frame) varies for the CAMTUNER-based VAP and the Baseline VAP.

We make the following observations. (1) Starting with the default camera parameter setting, *i.e.,* [50, 50, 50, 50], CAMTUNER decrements the sharpness parameter after looking into the initial two frames, and then decrements contrast after 7 tuning intervals (at 70$^{\text{th}}$ second). At the 13^{th} tuning interval, it increments a third parameter, brightness. Then again after two intervals (at 150$^{\text{th}}$ second), it increments the sharpness parameter. In the subsequent interval, CAMTUNER decides to decrement color-saturation after looking into the most recently captured scene. Finally, CAMTUNER further decrements the sharpness parameter three more times where the first two are separated by 10s but the last parameter change (at 270$^{\text{th}}$ second) happens after a 90s gap. Throughout the 5-minute video, CAMTUNER adjusts the camera setting 8 times. The camera setting adaption improves the mIoU per frame by 0.026 on average with the maximum mIoU improvement of 0.67 in comparison with using the default camera parameter setting. (2) CAMTUNER improves the mIoU for 24.8% of the video frames (by a maximum of 0.67) and only minimally reduces the mIoU for 1.6% of the frames (by a maximum of 0.005). An mIoU value of zero implies that no face in the input scene is detected by the face-detection AU. (3) Figure 13b also shows that while faces are not detected under the default setting for 2.4% of the frames, the face-detection AU can detect faces in those frames once CAMTUNER adapts the camera parameters.

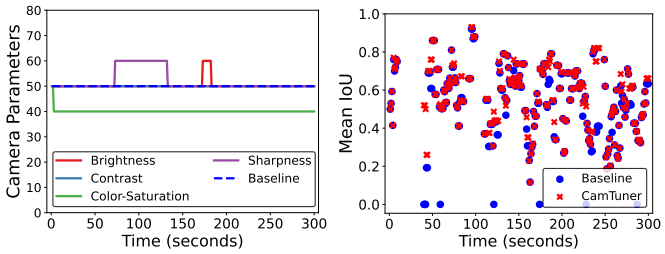

(a) Camera setting adaptation (b) mIoU variation

Fig. 14: *CamTuner* in operation during afternoon.

While Figure 13 illustrates CAMTUNER's reaction to environmental and content variations during the morning, Figure 14a showcases the adjustments to camera parameters during a different time-of-day, *i.e.,* afternoon, and their impact on face-detection accuracy, shown in Figure 14b in terms of mean IoU. Starting with the default camera parameter setting, *i.e.,* [50, 50, 50, 50], CAMTUNER only adjusts the camera setting 5 times throughout the 5-minute video during afternoon which is fewer than the adjustments recorded in the morning, also shown in Figure 13a. These adaptations improve the mIoU per frame by 0.037 on average with the maximum mIoU improvement of 0.55 compared to using the default camera parameter setting. Furthermore, CAMTUNER enhances the mean IoU for 41.2% of the video frames (by a maximum of 0.72) and minimally reduces the mean IoU for 1.7% of the frames (by a maximum of 0.003) during the randomly selected 5-minute period in the afternoon. Figures 13, 14 illustrate how diverse environmental conditions and content variations during different times of the day prompt CAMTUNER to adapt camera parameters accordingly, enhancing analytics accuracy.

B. How quickly does CAMTUNER *react to suboptimal settings*

Here, we evaluate how quickly CAMTUNER can react if the camera is set to a suboptimal setting that leads to degraded analytical outcome. We place two side-by-side cameras in front of a scene consisting of 3D objects as shown in Figure 15. In this scene, 3D slot cars are continuously moving over the track and 3D human models are kept stationary. Both cameras start with a same suboptimal setting (we use two suboptimal settings denoted as SS1 and SS2) and stream at 10 FPS for 2-minute period, during which the I-A parameters of Camera 1 are kept to the same initial suboptimal values, while the I-A parameters of Camera 2 are tuned by CAMTUNER every 2s. On every frame streamed from camera, we use Yolov5 [28] as the object detector to detect and record the type of objects with their bounding boxes [3]. Figure 16 plots the normalized moving average of the total number of object detections in the last 100 frames in the Y axis (to clearly show the trend) of the two cameras under two different initial suboptimal settings, SS1 and SS2. We observe a small initial gap between the performance of YOLOv5 between the two camera streams which indicates that within the first 10 seconds, CAMTUNER changes the camera parameters once based on analytics quality estimator output and achieves better object detection. Furthermore, we observe

[3]Manual inspection confirms no false-positive detection in the 2-minute period.

This article has been accepted for publication in IEEE Transactions on Mobile Computing. This is the author's version which has not been fully edited and content may change prior to final publication. Citation information: DOI 10.1109/TMC.2025.3540667

(a) capture under SS1 (b) capture under SS2 (c) CAMTUNER camera capture

Fig. 15: Sample static & CAMTUNER camera captures.

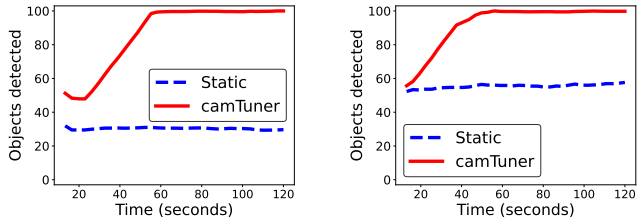

(a) suboptimal setting 1 (SS1) (b) suboptimal setting 2 (SS2)

Fig. 16: CAMTUNER reaction to suboptimal settings (Normalized Moving average of total object detection is computed over last 100 frames, shown in Y axis).

that CAMTUNER gradually converges to a best-possible setting within a minute that enables Yolov5 to detect all objects from the scene (total 5-7 more object detections per frame).

C. Real-world Deployment (Parking Lot)

To validate that similar accuracy improvement from video-playback in §VII-A2 is achieved in real-world deployment where the I-A parameters of the camera are continuously reconfigured by CAMTUNER, we evaluated our deployment of CAMTUNER at a large enterprise parking lot. The real-world deployment has two co-located cameras, as shown in Figure 17. One camera is part of the Baseline VAP (VAP 1) while the other camera is part of the CAMTUNER VAP (VAP 2). Both VAP deployments use Axis Q3505 MK II Network cameras, which upload the captured frames over 5G network to a remote edge-server (with a Xeon processor and an NVIDIA GPU) running the Efficientdet [50] object detection model to detect cars and persons in the parking lot. In VAP 2, the captured frames are also sent in parallel to CAMTUNER which runs on a low-end Intel-NUC box (with a 2.6 GHz Intel i7-6770HQ CPU). CAMTUNER is seeded with the same initially VC-trained RL agent as in §VII-A2 and it performs a few initial online exploration rounds and then starts exploitation and adjusts camera settings every 30 seconds. To evaluate the accuracy of the AUs in the VAPs, we ensure that both cameras view almost identical scenes at the same time.

We ran both VAPs side-by-side for 8 continuous hours in a day and recorded the videos from both VAPs. Since we want to manually inspect and validate the detections from both VAPs, we randomly picked detections for 5-minute spans during Morning and Evening time and compare car and person detections across the two VAPs. Figure 19 shows the cumulative number of true-positive car and person detections. Figure 19a and Figure 19c show that CAMTUNER detects 2.2% (3) and 15.9% (146) additional persons than Baseline during Morning and Evening, respectively. CAMTUNER also detects 2.6% (861) and 4.2% (881) more cars than the Baseline VAP during Morning and Evening, respectively, as shown in Figure 19b and Figure 19d. Upon manual inspection of the videos, we confirmed that CAMTUNER does not have any false positive detections for car/person. In appendix, we have also evaluated the performance of CAMTUNER for a 5G use-case.

Fig. 17: CAMTUNER real-world deployment setup.

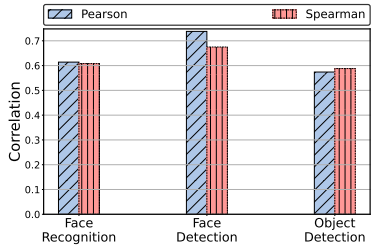

Fig. 18: Analytics quality estimator performance.

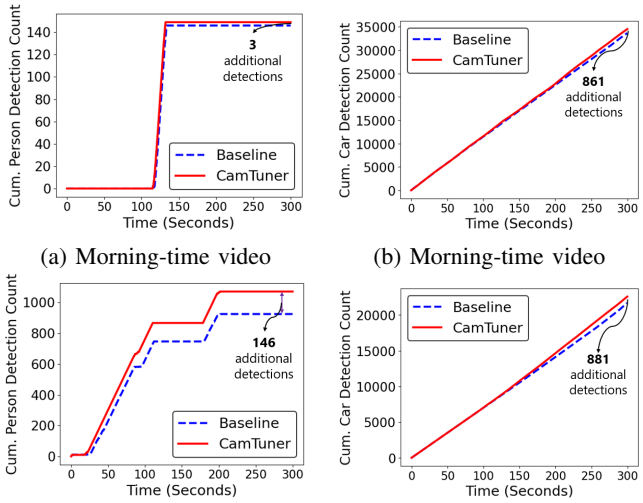

(a) Morning-time video (b) Morning-time video

(c) Evening-time video (d) Evening-time video

Fig. 19: CAMTUNER performance in Parking lot.

D. System Performance

Since CAMTUNER runs in parallel with the AU, it does not add any additional latency to the VAP and hence the AU latency. In the following, we show that the normal online operation of CAMTUNER is light-weight, and the initial training phase using VC can explore each action extremely fast.

First, during online operation, each iteration of CAMTUNER involves three tasks: evaluating the AU-specific quality estimator, evaluating the Q-function by the SARSA agent, and changing the parameters of the physical camera. We run CAMTUNER on a low-end edge device, an Intel-NUC box equipped with a 2.6 GHz Intel i7-6770HQ CPU. The AU-specific quality estimator takes 40ms on the Intel-NUC edge device, *i.e.,* 10X faster than the SOTA image classifiers, and the SARSA RL agent takes less than 1 ms to complete Q-function calculation and Q-table update. Since the two tasks can be pipelined with changing the physical camera settings which takes up to 200 ms on the AXIS Q3505 MK II Network camera we used, each iteration of CAMTUNER takes 200 ms, *i.e.,* 5 iterations per second, and the average CPU utilization is only 15% with 150 MB memory footprint.

Next, we run the initial RL training phase on a high-end PC with a 3.70 GHz Intel(R) Xeon(R) W-2145 CPU and GeForce RTX 2080 GPU. During the one-hour training phase performed

TABLE III: Accuracy of VC.

Parameter	Brightness	Contrast	Color -Saturation	Sharpness
Mean error	5.4 %	13.8 %	17.3 %	19.8 %
Std. dev.	1.7 %	4.3 %	9.6 %	8.1 %

in §VII-E, in each iteration of the RL exploration, VC takes 4 ms to output f_o, the quality estimator takes 10 ms, and the RL agent take less than 1 ms to evaluate the Q-function and update the Q-table, for a total of 15 ms. As a result, CAMTUNER can explore around 70 actions per second, which is 14X faster than using the physical camera. The CPU utilization in this case is steady at 60%.

E. Accuracy of Offline Trained Models

Finally, we evaluate the efficacy of two key components of CAMTUNER which are trained offline: VC and AU-specific analytics quality estimator model.

Virtual camera. VC is designed to render a frame taken at one time (T_1) to another time (T_2), as if the rendered frame were captured at time T_2. First, we trained VC in the offline profiling phase as discussed in §V-C using a 24-hour long video obtained from one of our customer locations at an airport. To evaluate how well VC works online, we obtained several video snippets at 6 different hours of the day from the same camera. Next, we fed 1 video snippet VS_0 from one particular hour H_0 through VC which applies different digital transformation to generate 5 video snippets VS_j corresponding to the hours of the other 5 videos. For each generated video snippet VS_j, we calculated the relative error of the metric tuple values of each frame in VS_j relative to that of the corresponding original video frame and average such error across all the frames in VS_j (over 37.5K frames). We collected 30 VC error tuples by repeating the experiment for six original video snippets, each corresponding to a different hour. Table III shows the mean error and standard deviation among all 30 VC error tuples. We observe that the average VC errors are *5.4%*, *13.8%*, *17.3%*, and *19.8%* for brightness, contrast, color-saturation, and sharpness respectively. Table III shows that the average VC errors for color-saturation and sharpness are significantly higher than for brightness. This is because brightness remains relatively stable over short periods (e.g., a 15-minute window), while other image metrics fluctuate more. Despite this variance, the results demonstrate that with preliminary camera virtualization, we can render the same frame at different times of day with an average error of less than 20%, which can accelerate SARSA RL exploration. Lower VC errors could improve the effectiveness of CAMTUNER's RL model in learning the best actions to take upon environmental changes, and improving virtual camera accuracy is a key area of future research.

We note that simulating different times alone may be insufficient for cameras deployed in diverse locations, especially when the locations vary significantly. Location-specific exploration of the CAMTUNER RL agent remains an area for future research.

AU-specific analytics quality estimator. This estimator is a lightweight model that predicts coarse-grained accuracy measure of the heavyweight DNN model (*i.e.,* used in AU), it is not meaningful to compare its accuracy against the accuracy achieved by the heavyweight model (derived using ground truth). Thus, we evaluated the quality of the AU-specific quality estimator by measuring the Spearman and Pearson correlation between the two accuracies for three different AUs i.e. face-recognition, face-detection, and person-detection. First, we trained the three estimators through supervised learning as described in Section V-B. To evaluate the face-recognition estimator, we used the celebA-validation dataset which contains 200 images (*i.e.,* different from the 300 original training images used in Section V-B) and their about 2 million variants from augmenting the original images using the python-pil image library [13]. Figure 18 shows that the quality predicted by the face-recognition analytics quality estimator is strongly correlated with the output by the AU (both Pearson and Spearman correlation are greater than 0.6) [47], [8].

To evaluate the face-detection quality estimator, we used annotated video frames from the *olympics* [39] and *HMDB* datasets [33] along with their 4 million generated variants. To evaluate object-detection analytics quality estimator, we used labelled images (*i.e.,* only consist car and person object classes) from the COCO dataset [35] and their 7 million augmented variants Figure 18 shows that there is a strong positive correlation between the measured mAP and IoU metric and the predicted quality estimate for both face-detection and object-detection AUs. Such a high correlation between the AU-specific analytics quality estimator's predictions and the heavy-weight DNN's predictions suggests that our lightweight model effectively captures the heavy-weight DNN's perception, which significantly boosts CAMTUNER's adaptability to external environmental changes.

VIII. RELATED WORK

Similar to our findings, Jang *et al.* [26] also observe the impact of environmental conditions on VAP, but they propose adapting different AUs based on these conditions. However, developing AUs for every environmental scenario is impractical. In contrast, CAMTUNER maintains a fixed AU while adjusting camera settings to accommodate environmental changes.

Several works investigate tuning parameters of a VAP after camera capture and before sending it to an AU or changing the AU based on the input video content. Videostorm [57], Chameleon [27], and Awstream [56] tune the after-capture video stream parameters such as frames-per-second or frame resolution to ensure efficient resource usage while processing video analytics queries at scale. In contrast, CAMTUNER dynamically tunes camera parameters to improve the AU accuracy of VAPs.

Recent studies, *e.g.,* Focus [24], NoScope [29], Ekya [41], and AMS [30], explored adapting AU model parameters based on captured video content, necessitating additional GPU resources for periodic model retraining showing less reactivity to video content changes. In contrast, CAMTUNER quickly adapts camera parameters in real-time to environmental changes.

Several frame filtering techniques on edge devices [9], [43], [11], [34] are complementary to CAMTUNER. While CAMTUNER's AU-specific analytics quality estimator focuses on

This article has been accepted for publication in IEEE Transactions on Mobile Computing. This is the author's version which has not been fully edited and content may change prior to final publication. Citation information: DOI 10.1109/TMC.2025.3540667

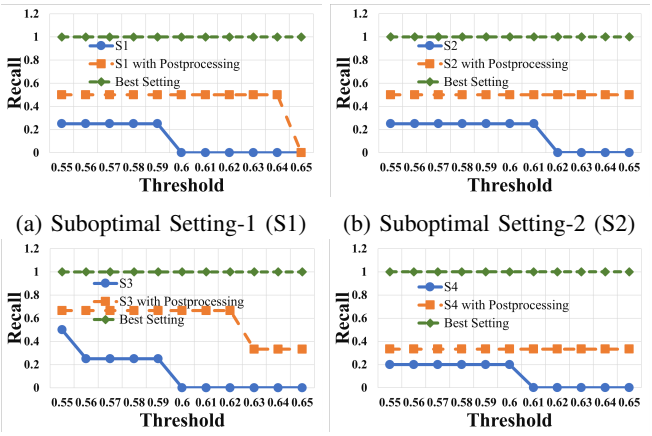

(a) Suboptimal Setting-1 (S1) (b) Suboptimal Setting-2 (S2)

(c) Suboptimal Setting-3 (S3) (d) Suboptimal Setting-4 (S4)

Fig. 20: Parameter tuning vs. *postprocessing* for NIGHT.

quality estimation tailored to each AU, AQuA's estimator [43] performs coarse-grained, AU-agnostic image quality estimation.

There is a large body of work on configuring the Image Signal Processing pipeline (ISP) in cameras to improve human-perceived quality of images from the cameras [54], [36], [19], [40], [55]. In contrast, we study dynamic camera parameter tuning to optimize the accuracy of VAPs.

Recent works like MadEye [53] and AcTrak [20] concentrate on tuning PTZ cameras. MadEye [53] autonomously adjusts camera orientations through periodic searches in a vast orientation space, while AcTrak [20] employs RL to dynamically zoom in on targets and detect new arrivals in the scene.Two recent works focus on tuning PTZ cameras.

IX. Discussion

In addition to dynamically tuning network camera parameters before frame capture, CamTuner can also determine optimal digital transformations for post-capture processing, especially for cameras that do not expose REST APIs for remote camera parameter tuning. However, it is important to note that adjusting camera parameters for better image or video capture is fundamentally different from applying post-capture transformations. To evaluate this, we observed the performance of a face recognition AU (Neoface-v3) under four different sub-optimal camera settings (S1, S2, S3, S4) during NIGHT conditions following the same experimental setup described in III-B.

Figure 20 compares the results of actual camera parameter tuning and post-capture transformations. The initial frames were of poor quality, resulting in low Recall (true-positive rate) across all settings. After applying digital transformations to these frames, Recall improved but remained suboptimal. In contrast, directly tuning the camera to the "best setting" achieved a perfect Recall (*i.e.,* 100%). These results indicate that while post-capture transformations can enhance capture quality, they are limited compared to direct camera parameter tuning, which not only yields better accuracy of analytics but also reduces end-to-end latency.

X. Future Work

In future work, we will explore a broader spectrum of environmental influences and external factors beyond CamTuner's four primary NAUTO image-appearance parameters.

(a) Vibration of sensor (b) Sensor heating up

Fig. 21: Camera misconfigurations and its visual impacts.

Use cases that require diagnosis and camera tuning. There are potentially many usecases of VAP deployments that require diagnosis and camera parameter adjustments. For instance, external factors such as camera vibration due to environmental conditions can induce motion blur, as depicted in Figure 21a. This can be mitigated through anti-vibration mounts or adjusting the stabilizer parameter in the camera. Additionally, unsynchronized object movement with camera shutter speed can further induce motion blur. Furthermore, variations in voltage and illumination may lead to sensor heating, adding Gaussian noise to the capture, as illustrated in Figure 21b. Such occurrences may also impede the generation of specific on-camera alerts if the camera sensor and processing device become overheated, causing CPU throttling. Diagnosing such issues and providing feedbacks to tune camera parameters accordingly can markedly enhance the accuracy of VAPs.

Tuning other NAUTO parameters. While our initial demonstration in this paper focuses only on a subset of NAUTO camera parameters related to image appearance, there are several other NAUTO parameters such as max exposure time, maximum gain, defog effect (listed in Table I) that can be dynamically tuned to enhance video analytics accuracy. While image appearance parameters (*e.g.,* brightness, contrast, color level, and sharpness) individually influence a single perceived metric, exposure settings not only determine the brightness of a captured image but also affect depth of field, motion blur, sharpness of moving content, and image noise. On the other hand, video stream-specific parameters such as frame resolution target bitrate, and GOP length impact both the size and quality of the output frame or video stream. In our future work, we plan to study the impact of dynamically tuning these other camera parameters as well.

Finally, CamTuner's dynamic tuning methodology can be used to automatically and dynamically tune other complex sensors such as depth and thermal cameras. In the appendix, we demonstrate the superiority of modifying in-camera parameters over applying post-capture digital transformations and discuss the potential extension of our approach to finding optimal post-capture parameters.

XI. Conclusion

In this paper, we presented the design and assessment of CamTuner, to our knowledge the first VAP framework that enhances AU accuracy by dynamically learning the optimal settings for NAUTO camera parameters deployed in real-world scenarios. CamTuner's design and its key components, *Virtual Camera* and *light-weight AU-specific analytics quality estimators*, can be applied to dynamically tune many other non-automated (NAUTO) parameters of cameras as well as other complex sensors such as depth and thermal cameras.

REFERENCES

[1] NATS: Connective Technology for Adaptive Edge & Distributed Systems. https://nats.io/.

[2] Open Source Computer Vision Library. https://opencv.org/.

[3] Zeromq: An open-source universal messaging library. https://zeromq.org/.

[4] Vp9. https://www.webmproject.org/vp9/, 2017.

[5] x264. http://www.videolan.org/developers/x264.html, 2021.

[6] B. E. Bayer. Color imaging array, July 20 1976. US Patent 3,971,065.

[7] S. Bezryadin, P. Bourov, and D. Ilinih. Brightness calculation in digital image processing. In *International symposium on technologies for digital photo fulfillment*, volume 2007, pages 10–15. Society for Imaging Science and Technology, 2007.

[8] T. BMJ. correlation-and-regression. https://www.bmj.com/about-bmj/resources-readers/publications/statistics-square-one/11-correlation-and-regression, 2019.

[9] C. Canel, T. Kim, G. Zhou, C. Li, H. Lim, D. G. Andersen, M. Kaminsky, and S. Dulloor. Scaling Video Analytics on Constrained Edge Nodes. In A. Talwalkar, V. Smith, and M. Zaharia, editors, *Proceedings of Machine Learning and Systems*, volume 1, pages 406–417, 2019.

[10] E. H. Chen, P. Röthig, J. Zeisler, and D. Burschka. Investigating Low Level Features in CNN for Traffic Sign Detection and Recognition. In *2019 IEEE Intelligent Transportation Systems Conference (ITSC)*, pages 325–332, 2019.

[11] T. Y.-H. Chen, L. Ravindranath, S. Deng, P. Bahl, and H. Balakrishnan. Glimpse: Continuous, real-time object recognition on mobile devices. In *Proceedings of the 13th ACM Conference on Embedded Networked Sensor Systems*, pages 155–168, 2015.

[12] CISCO. Cisco Video Surveillance IP Cameras. https://www.cisco.com/c/en/us/products/physical-security/video-surveillance-ip-cameras/index.html.

[13] A. Clark and Contributors. Pillow library. https://pillow.readthedocs.io/en/stable/.

[14] CNET. How 5G aims to end network latency. CNET_5G_network_latency_time, 2019.

[15] cocoapi github. pycocotools. https://github.com/cocodataset/cocoapi/tree/master/PythonAPI/pycocotools.

[16] A. Communication. AXIS Network Cameras. https://www.axis.com/products/network-cameras.

[17] K. De and V. Masilamani. Image sharpness measure for blurred images in frequency domain. *Procedia Engineering*, 64:149–158, 2013.

[18] J. Deng, J. Guo, Z. Yuxiang, J. Yu, I. Kotsia, and S. Zafeiriou. RetinaFace: Single-stage Dense Face Localisation in the Wild. In *arxiv*, 2019.

[19] S. Diamond, V. Sitzmann, F. Julca-Aguilar, S. Boyd, G. Wetzstein, and F. Heide. Dirty Pixels: Towards End-to-end Image Processing and Perception. *ACM Transactions on Graphics (TOG)*, 40(3):1–15, 2021.

[20] A. Fahim, E. Papalexakis, S. V. Krishnamurthy, A. K. Roy Chowdhury, L. Kaplan, and T. Abdelzaher. Actrak: Controlling a steerable surveillance camera using reinforcement learning. *ACM Transactions on Cyber-Physical Systems*, 7(2):1–27, 2023.

[21] V. Gaikwad and R. Rake. Video Analytics Market Statistics: 2027, 2021.

[22] A. Gupta, A. Anpalagan, L. Guan, and A. S. Khwaja. Deep learning for object detection and scene perception in self-driving cars: Survey, challenges, and open issues. *Array*, 10:100057, 2021.

[23] D. Hasler and S. E. Suesstrunk. Measuring colorfulness in natural images. In *Human vision and electronic imaging VIII*, volume 5007, pages 87–95. International Society for Optics and Photonics, 2003.

[24] K. Hsieh, G. Ananthanarayanan, P. Bodik, S. Venkataraman, P. Bahl, M. Philipose, P. B. Gibbons, and O. Mutlu. Focus: Querying Large Video Datasets with Low Latency and Low Cost. In *13th USENIX Symposium on Operating Systems Design and Implementation (OSDI 18)*, pages 269–286, Carlsbad, CA, Oct. 2018. USENIX Association.

[25] i PRO. i-PRO Network Camera. http://i-pro.com/global/en/surveillance.

[26] S. Y. Jang, Y. Lee, B. Shin, and D. Lee. Application-Aware IoT Camera Virtualization for Video Analytics Edge Computing. *2018 IEEE/ACM Symposium on Edge Computing (SEC)*, pages 132–144, 2018.

[27] J. Jiang, G. Ananthanarayanan, P. Bodik, S. Sen, and I. Stoica. Chameleon: scalable adaptation of video analytics. In *Proceedings of the 2018 Conference of the ACM Special Interest Group on Data Communication*, pages 253–266, 2018.

[28] G. Jocher, A. Chaurasia, A. Stoken, J. Borovec, NanoCode012, Y. Kwon, TaoXie, J. Fang, imyhxy, K. Michael, Lorna, A. V, D. Montes, J. Nadar, Laughing, tkianai, yxNONG, P. Skalski, Z. Wang, A. Hogan, C. Fati, L. Mammana, AlexWang1900, D. Patel, D. Yiwei, F. You, J. Hajek, L. Diaconu, and M. T. Minh. ultralytics/yolov5: v6.1 - TensorRT, TensorFlow Edge TPU and OpenVINO Export and Inference, Feb. 2022.

[29] D. Kang, J. Emmons, F. Abuzaid, P. Bailis, and M. Zaharia. NoScope: Optimizing Neural Network Queries over Video at Scale. *Proc. VLDB Endow.*, 10(11):1586–1597, Aug. 2017.

[30] M. Khani, P. Hamadanian, A. Nasr-Esfahany, and M. Alizadeh. Real-Time Video Inference on Edge Devices via Adaptive Model Streaming. *arXiv preprint arXiv:2006.06628*, 2020.

[31] D. P. Kingma and J. Ba. Adam: A method for stochastic optimization. *arXiv preprint arXiv:1412.6980*, 2014.

[32] A. Krizhevsky, I. Sutskever, and G. E. Hinton. Imagenet classification with deep convolutional neural networks. In *Advances in neural information processing systems*, pages 1097–1105, 2012.

[33] H. Kuehne, H. Jhuang, E. Garrote, T. Poggio, and T. Serre. HMDB: a large video database for human motion recognition. In *Proceedings of the International Conference on Computer Vision (ICCV)*, 2011.

[34] Y. Li, A. Padmanabhan, P. Zhao, Y. Wang, G. H. Xu, and R. Netravali. Reducto: On-Camera Filtering for Resource-Efficient Real-Time Video Analytics. In *Proceedings of the Annual conference of the ACM Special Interest Group on Data Communication on the applications, technologies, architectures, and protocols for computer communication*, pages 359–376, 2020.

[35] T.-Y. Lin, M. Maire, S. Belongie, J. Hays, P. Perona, D. Ramanan, P. Dollár, and C. L. Zitnick. Microsoft coco: Common objects in context. In *European conference on computer vision*, pages 740–755. Springer, 2014.

[36] L. Liu, X. Jia, J. Liu, and Q. Tian. Joint demosaicing and denoising with self guidance. In *Proceedings of the IEEE/CVF Conference on Computer Vision and Pattern Recognition*, pages 2240–2249, 2020.

[37] Z. Liu, P. Luo, X. Wang, and X. Tang. Deep Learning Face Attributes in the Wild. In *Proceedings of International Conference on Computer Vision (ICCV)*, December 2015.

[38] A. Mittal, A. K. Moorthy, and A. C. Bovik. No-reference image quality assessment in the spatial domain. *IEEE Transactions on image processing*, 21(12):4695–4708, 2012.

[39] J. C. Niebles, C.-W. Chen, and L. Fei-Fei. Modeling temporal structure of decomposable motion segments for activity classification. In *European conference on computer vision*, pages 392–405. Springer, 2010.

[40] J. Nishimura, T. Gerasimow, S. Rao, A. Sutic, C.-T. Wu, and G. Michael. Automatic ISP image quality tuning using non-linear optimization, 2019.

[41] A. Padmanabhan, A. P. Iyer, G. Ananthanarayanan, Y. Shu, N. Karianakis, G. H. Xu, and R. Netravali. Towards Memory-Efficient Inference in Edge Video Analytics.

[42] M. N. Patrick Grother and K. Hanaoka. Face Recognition Vendor Test (FRVT). https://nvlpubs.nist.gov/nistpubs/ir/2019/NIST.IR.8271.pdf, 2019.

[43] S. Paul, U. Drolia, Y. C. Hu, and S. T. Chakradhar. Aqua: Analytical quality assessment for optimizing video analytics systems. In *2021 IEEE/ACM Symposium on Edge Computing (SEC)*, pages 135–147. IEEE, 2021.

[44] E. Peli. Contrast in complex images. *JOSA A*, 7(10):2032–2040, 1990.

[45] Qualcomm. How 5G low latency improves your mobile experiences. Qualcomm_5G_low-latency_improves_mobile_experience, 2019.

[46] R. Ramanath, W. E. Snyder, Y. Yoo, and M. S. Drew. Color image processing pipeline. *IEEE Signal Processing Magazine*, 22(1):34–43, 2005.

[47] Statisticssolutions. Pearson correlation coefficient. https://www.statisticssolutions.com/free-resources/directory-of-statistical-analyses/pearsons-correlation-coefficient/, 2019.

[48] R. S. Sutton, A. G. Barto, et al. *Introduction to reinforcement learning*, volume 135. MIT press Cambridge, 1998.

[49] C. Szegedy, V. Vanhoucke, S. Ioffe, J. Shlens, and Z. Wojna. Rethinking the Inception Architecture for Computer Vision. In *2016 IEEE Conference on Computer Vision and Pattern Recognition (CVPR)*, pages 2818–2826, 2016.

[50] M. Tan, R. Pang, and Q. V. Le. Efficientdet: Scalable and efficient object detection. In *Proceedings of the IEEE/CVF conference on computer vision and pattern recognition*, pages 10781–10790, 2020.

[51] C. J. C. H. Watkins and P. Dayan. Q-learning. In *Machine Learning*, pages 279–292, 1992.

[52] M. Wiering and J. Schmidhuber. Fast Online q(λ). *Machine Learning*, 33(1):105–115, Oct 1998.

[53] M. Wong, M. Ramanujam, G. Balakrishnan, and R. Netravali. Madeye: Boosting live video analytics accuracy with adaptive camera configurations. *arXiv preprint arXiv:2304.02101*, 2023.

[54] C.-T. Wu, L. F. Isikdogan, S. Rao, B. Nayak, T. Gerasimow, A. Sutic, L. Ain-kedem, and G. Michael. VisionISP: Repurposing the image signal processor for computer vision applications. In *2019 IEEE International Conference on Image Processing (ICIP)*, pages 4624–4628. IEEE, 2019.

[55] F. Xu, Z. Liu, Y. Lu, S. Li, S. Xu, Y. Fan, and Y.-K. Chen. Ai-assisted isp hyperparameter auto tuning. In *2023 IEEE 5th International Conference on Artificial Intelligence Circuits and Systems (AICAS)*, pages 1–5, 2023.

[56] B. Zhang, X. Jin, S. Ratnasamy, J. Wawrzynek, and E. A. Lee. Awstream: Adaptive wide-area streaming analytics. In *Proceedings of the 2018 Conference of the ACM Special Interest Group on Data Communication*, pages 236–252, 2018.

[57] H. Zhang, G. Ananthanarayanan, P. Bodik, M. Philipose, P. Bahl, and M. J. Freedman. Live Video Analytics at Scale with Approximation and Delay-Tolerance. In *14th USENIX Symposium on Networked Systems Design and Implementation (NSDI 17)*, pages 377–392, Boston, MA, Mar. 2017. USENIX Association.

Sibendu Paul is an applied scientist at Amazon Prime Video Team. He earned his Ph.D. in Electrical and Computer Engineering from Purdue University in 2022, where he received the Bilsland Dissertation Fellowship. His research encompasses mobile systems, computer vision, video analytics, AR/VR systems and machine learning systems, with publications in esteemed conferences like ACM HotMobile, Sensys, ASPLOS, and INFOCOM *etc.* Furthermore, he holds three granted patents and was awarded the University Gold Medal during his undergraduate studies at Jadavpur University.

Kunal Rao is a researcher in the Integrated Systems Department at NEC Laboratories America, Inc. in Princeton, NJ. He has received a Master's degree in Electrical and Computer Engineering from University of Florida, Gainesville. His research interests have revolved around High Performance Computing (HPC), Heterogeneous Cluster Computing, GPGPU Computing, Xeon Phi Computing, Graph Computing and Graph Analytics, and more recently into Distributed Real-time Stream Processing Systems for AI-powered video analytics solutions, and application of AI/ML techniques to solve systems problems. Kunal has received several business contribution and spot recognition awards at NEC Laboratories America, Inc. and has over 20 publications in top tier IEEE/ACM conferences and over 20 granted patents.

Giuseppe Coviello is a researcher in the Integrated Systems Department at NEC Laboratories America, Inc. in Princeton, NJ. He has been working in the "computing" environment since 2003. He has started as a hobbyist and contributed to many Open Source projects liken CRUX, a GNU/Linux distributions, the Linux kernel, Fedora Linux. He got a BS degree in Computer Science in 2010. His main research interests are related to the operating systems, the high performance computing, the cloud computing. In all of those years of hobby, study and research he built a very good knowledge about the internals of Linux, starting from the kernel to the system administration and to the software development.

Murugan Sankaradas is a Senior Researcher in NEC Laboratories America, whose research interests lie in video analytics, vision language models, 5G networks, and edge computing. His patents and publications portfolio span a wide range of topics, including stream processing, microservices, resource management, machine learning, deep learning and data processing.

Y. Charlie Hu (Fellow, IEEE) received the Ph.D. degree in computer science from Harvard University in 1997. From 1997 to 2001, he was a Research Scientist at Rice University. He is currently a Michael and Katherine Birck Professor of ECE with Purdue University. His research interests include mobile computing, operating systems, distributed systems, and wireless networking. He has published over 180 papers in these areas. He received the NSF CAREER Award in 2003. He is an ACM Distinguished Scientist.

Dr. Srimat Chakradhar is a Department Head at NEC Laboratories America, Princeton, NJ. He has over thirty years of experience in AI, machine learning, video analytics, digital transformation, distributed computing, 5G networking, and embedded systems in domestic and global sectors. He is a hands-on leader with proven track record of success in designing and delivering several commercially successful, award-winning innovative AI solutions, services and products. Dr. Chakradhar is a Fellow of the IEEE.